Direct atomic structure determination of epitaxially grown films: Gd_2O_3 on GaAs(100)

M. Sowwan and Y. Yacoby*
Racah Institute of Physics, Hebrew University, Jerusalem, 91904 Israel

J. Pitney, R. MacHarrie, and M. Hong
Bell Laboratories, Lucent Technologies, 700 Mountain Ave, Murray Hill, New Jersey 07974

J. Cross
PNC-CAT, Advanced Photon Source, Argonne National Laboratory, Argonne, Illinois 60439

D. A. Walko
MHATT-CAT, Advanced Photon Source, Argonne National Laboratory, Argonne, Illinois 60439

R. Clarke
NSF FOCUS Center, Department of Physics, University of Michigan, Ann Arbor, Michigan 48109-1120

R. Pindak
National Synchrotron Light Source, Brookhaven National Laboratory, Upton, New York 11973

E. A. Stern
Physics Department, University of Washington Seattle Washington, 98195-1560
(Received 5 June 2002; revised manuscript received 29 August 2002; published 8 November 2002)

We have used coherent bragg rod analysis (COBRA) to investigate the atomic structure of an epitaxial Gd_2O_3 film grown on a (100) GaAs substrate. COBRA is a method to directly obtain the structure of systems periodic in two dimensions by determining the complex scattering factors along the substrate-defined Bragg rods. The system electron density and atomic structure are obtained by Fourier transforming the complex scattering factors into real space. The results show that the stacking order of the Gd_2O_3 film layers is different from that of cubic bulk Gd_2O_3 and resembles the stacking order of Ga and As layers in GaAs. Furthermore, in the first few Gd_2O_3 layers, Gd atoms are displaced to positions right above the Ga and As positions in the substrate, and they relax towards bulk Gd_2O_3 positions with increasing distance from the interface.

DOI: 10.1103/PhysRevB.66.205311 PACS number(s): 68.55.−a, 61.10.Kw

I. INTRODUCTION

Epitaxially grown thin films have emerged as a class of materials whose properties often differ substantially from those of the corresponding bulk materials. Such films form the basis of much of current electronics technology. As device dimensions shrink to nanometer levels, and novel nanofabricated composite structures are explored, the interface region between the film and the substrate on which it is grown takes on an increasingly important role.

Obtaining accurate structural information at interfaces is nowhere more critical than in semiconductor passivation layers, where details of the atomic structure and bonding determine the nature of the interface electronic states. In this paper we report the results of a study of the structure of a recently discovered passivation layer for GaAs: epitaxially grown Gd_2O_3. We have been able to achieve an unprecedented level of detail in the atomic structure by using the diffraction technique coherent bragg rod analysis (COBRA)[1] which is especially sensitive to the arrangement of atoms in epitaxial films and interfaces. There have been many attempts over the past 30 years to find an insulating layer that will passivate the GaAs (100) surface.[2–8] Most of the attempts have failed either because the interfacial state density was unacceptably high, or because the layers were not thermodynamically stable relative to the GaAs interface. This is a particularly difficult problem for III-V compound semiconductors on account of their reactive nature and the relatively high mobility of the group V species in this family of compounds.

A promising direction was initiated by Hong *et al.*[9] in their studies of $(Ga_2O_3)_{1-x}/(Gd_2O_3)_x$ -GaAs interfaces, showing that while pure Ga_2O_3 does not passivate GaAs, the mixed oxide is electrically insulating with high electrical breakdown strength if $x>14\%$. These results pointed the way to Gd_2O_3 as an effective dielectric layer for the passivation of GaAs. Subsequent studies[10] confirmed that Gd_2O_3 is indeed potentially useful as a passivation layer exhibiting a midgap interfacial state density of as little as 10^{11} cm^{-2} eV^{-1}, only slightly higher than that of Si-SiO_2 interfaces. With a dielectric constant of 10, this oxide is an excellent dielectric with leakage current densities in the range 10^{-9}–10^{-10} A/cm^2, showing much promise as a passivation layer. Gd_2O_3 and Y_2O_3 films are also viewed as potential high dielectric constant passivation layers for Si. However, the reason for such a remarkably low interfacial state density is not understood at this time.

The first step in understanding the properties of any ma-

terial system usually begins with its atomic structure. However, little is known about the detailed atomic structure at buried interfaces on account of the lack of appropriate nondestructive techniques which could provide the statistical information needed for the theoretical modeling of their properties. This difficulty arises because interface structures are complicated. The atomic positions may be different in each layer of the structure, so that in general the three-dimensional crystal translational symmetry is reduced to two-dimensional periodicity in the plane of the film with the aperiodic structure in the perpendicular direction varying throughout the entire film thickness. We refer to this situation as a two-dimensional (2D) crystal. Various techniques have been used to investigate the atomic structure of epitaxially grown films. These include high resolution transmission electron microscopy,[11] x-ray absorption fine structure (XAFS),[12] diffuse x-ray scattering,[13] x-ray reflectivity,[14] x-ray standing waves,[15] x-ray diffraction along Bragg and truncation rods,[16] channeling,[17] and x-ray holography.[18] Some of these techniques have been used to investigate the structure of the Gd_2O_3 films. Kortan *et al.*[19] found that films grown under conditions similar to those of our sample grow as a single cubic crystal with Gd_2O_3 $\langle 110 \rangle$ perpendicular to the GaAs (100) substrate surface, Gd_2O_3 $\langle 001 \rangle$ parallel to GaAs $\langle 011 \rangle$ and the orthogonal Gd_2O_3 $\langle 1-10 \rangle$ axis coinciding with the GaAs $\langle 0-11 \rangle$. The film has 180° rotation symmetry but no 90° rotation and is single domain. Secondary electron imaging has confirmed these results.[20] XAFS measurements[12] have shown that the Gd-oxygen bonds increase by 2.7% +/- 0.6% relative to the bulk and this increase is consistent with the observed expansion in the lattice spacing perpendicular to the interface. Generally, all these techniques provide important information but they all suffer from one or both of the following limitations.

(a) Obtaining reliable structural information requires a correct structural model with parameters that can be refined by comparing the experimental results to the predictions of the model.

(b) The structural information provided is an average over inequivalent probe positions.

Both limitations are severe when dealing with epitaxial layers. Guessing the correct structural model for an epitaxial layer may be very difficult because of its complexity. In addition, probe atoms of the same species are often located at many inequivalent positions.

The COBRA technique we have used for this study overcomes these limitations because it is a direct method of structure determination, utilizing the high degree of transverse coherence of x-ray beams from an insertion device.[1] Most importantly, by measuring the diffraction intensities along substrate-defined Bragg rods, COBRA is able to extract the phase of the complex structure factor and hence obtain the three-dimensional electron density distribution by Fourier transformation.

A number of attempts have been made to solve the general phase problem for systems with 2D periodicity. Torrelles *et al.*[21] developed a method based on the Rius *et al.*[22] tangent formula for obtaining the structure of reconstructed surfaces. Recently, this method was used to study the structure of C_{60} on Au crystals with a resolution of about 1.9 Å.[23] Another method has been recently proposed by Saldin *et al.*[24] This method is based on the Bayes theorem and the maximum entropy approach. Both methods lead to recursion formulas that are quite cumbersome and require a very large number of iterations to obtain convergence, which is not always achieved. In contrast, COBRA requires only a very small number or no iterations at all. Our method can therefore handle complicated structures with very large numbers of atoms per 2D unit cell. We shall demonstrate that the results obtained provide very detailed and quite surprising new information on the structure of the GaAs:Gd_2O_3 system.

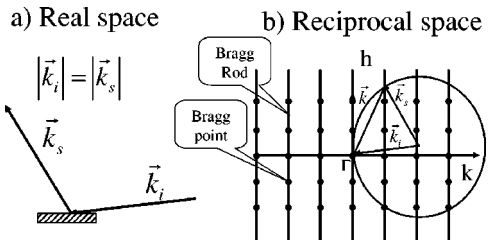

FIG. 1. (a) Scattering geometry: The incident beam with a wave vector k_i impinges on the sample surface. The sample is centered on a six circle goniometer. The scattered beam intensity with a wave vector k_s is measured by the detector mounted on the detector arm of the goniometer. (b) Reciprocal space representation of the scattering geometry: The dots represent the GaAs reciprocal lattice points. The vertical lines represent Bragg rods. The circle represents the Ewald sphere. The three arrows represent incident k_i the scattered k_s and the crystal momentum transfer k.

This paper is structured as follows. In Sec. II we provide an outline of the COBRA method. In Sec. III we discuss the sample preparation and characterization. Sec. IV presents the experimental aspects of this work followed by the results in Sec. V. In Sec. VI we provide a detailed account of the analysis. The structural implications of the electron density maps are discussed in Sec. VII. Lastly, Sec. VIII summarizes the results and presents conclusions with respect to the COBRA method in general, and to the GaAs:Gd_2O_3 system in particular.

II. THE COBRA METHOD

We present here an overview of the structure determination method in the optimized way it was applied to the GaAs:Gd_2O_3 system based on the method that has been presented by Yacoby *et al.*[1] To simplify the discussion we first assume that the epitaxial film has 2D periodicity with a period equal to that of the underlying substrate. The Fourier transform of the electron density of this system has the form of 2D delta functions in reciprocal space known as Bragg rods with superimposed 3D delta functions due to the 3D periodic electron density of the underlying crystal. The reciprocal lattice and the scattering conditions are schematically illustrated in Fig. 1.

The complex scattering factors (CSFs) along the Bragg rods contains all the information on the structure of this 2D crystal and the electron density can be obtained by Fourier transforming the CSF into real space. In a general sense the

total scattering intensity can be considered as coherently composed of two contributions: the scattering of a known reference electron density and that of an unknown electron density such that the combination of the two yields the scattering of the electron density of the real system. The reference part can be, for example, the known substrate and a simple model of the film. In this case the unknown electron density will be large within the film and the region of the substrate deformed by the film. At any two adjacent points along a Bragg rod differing by $\Delta\vec{k}$

$$S\left(\vec{k}-\frac{\Delta\vec{k}}{2}\right)+U\left(\vec{k}-\frac{\Delta\vec{k}}{2}\right)=T\left(\vec{k}-\frac{\Delta\vec{k}}{2}\right), \tag{1}$$

$$S\left(\vec{k}+\frac{\Delta\vec{k}}{2}\right)+U\left(\vec{k}+\frac{\Delta\vec{k}}{2}\right)=T\left(\vec{k}+\frac{\Delta\vec{k}}{2}\right), \tag{2}$$

where, S, U, and T are the complex scattering factors due to the reference, unknown, and total electron densities, respectively.

We now make use of the fact that the complex scattering factors vary continuously along the Bragg rods and make the approximation that at two adjacent points along a Bragg rod:

$$U\left(\vec{k}-\frac{\Delta\vec{k}}{2}\right)\approx U\left(\vec{k}+\frac{\Delta\vec{k}}{2}\right)=U_a(\vec{k}). \tag{3}$$

This approximation is valid if $U(\vec{k})$ varies slowly relative to $S(\vec{k})$. Taking the absolute value of Eqs. (1),(2) in this approximation yields

$$\left|S\left(\vec{k}-\frac{\Delta\vec{k}}{2}\right)+U_a(\vec{k})\right|=\left|T\left(\vec{k}-\frac{\Delta\vec{k}}{2}\right)\right|, \tag{4}$$

$$\left|S\left(\vec{k}+\frac{\Delta\vec{k}}{2}\right)+U_a(\vec{k})\right|=\left|T\left(\vec{k}+\frac{\Delta\vec{k}}{2}\right)\right|. \tag{5}$$

In Eqs. (4),(5) the absolute values squared of the total scattering factors are proportional to the experimentally determined intensity. This yields two real equations that can be solved for one complex unknown. In general this pair of equations has two solutions and it is necessary to choose the correct one. The correct solutions are obtained by looking at two pairs of equations at two consecutive pairs of points. This is shown in Fig. 2. The figure on the left represents the equations at $\vec{k}-\Delta\vec{k}/2$ and $\vec{k}+\Delta\vec{k}/2$. The corresponding complex numbers are marked with indices 1 and 2, respectively. The figure on the right represents the equations at $\vec{k}+\Delta\vec{k}/2$ and $\vec{k}+3\Delta\vec{k}/2$ and the corresponding indices are 2 and 3, respectively. Each pair of equations has two solutions U_a and U_b shown as solid and dashed lines, respectively. Under the assumption that U varies slowly along the Bragg rods the correct pair of solutions are the ones that change the least when going from one point to the next; namely, (in Fig. 2) U_{1a} and U_{2a}. This procedure then provides the unknown complex scattering factors and the complex total scattering factors along each Bragg rod. To obtain the electron density we Fourier transform the complex scattering factors into real space.

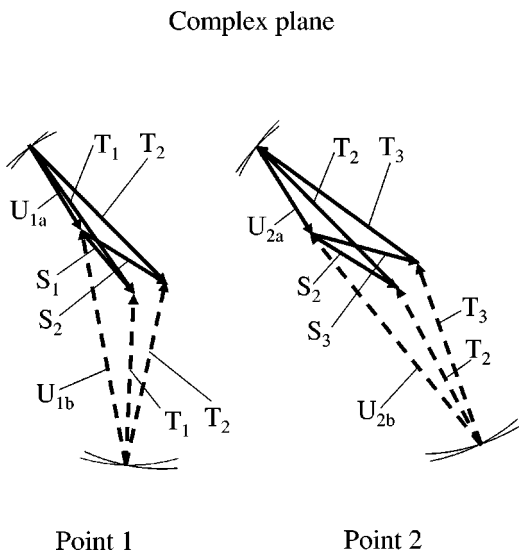

FIG. 2. Graphic representation of Eqs. (1) and (2) in the complex plane. The equations are shown for two pairs of adjacent points. S_1, S_2 and S_3 are the known complex scattering factors at $\vec{k}-\Delta\vec{k}/2$,$\vec{k}+\Delta\vec{k}/2$ and $\vec{k}+3\Delta\vec{k}/2$, respectively. The total scattering factors T are known only in absolute value so they are represented by arrows and arcs. U_{1a},U_{1b},U_{2a} and U_{2b} are two pairs of solutions. The correct solutions are those that vary the least when going from point 1 to point 2. Namely, in this case U_{1a} and U_{2a}.

The approximation made in Eq. (3) is justified if the rate of change of the reference scattering factor along the Bragg rod is larger than that of the unknown one. This is accomplished by a combination of two means. First, we choose the reference electron density to be similar to the electron density of the real system so that their scattering factors are of the same order of magnitude. Second, we use one of the properties of Fourier transformations, namely, that shifting the coordinate system origin in real space changes the rate of phase change in reciprocal space. We therefore place the origin of the real space coordinate system to be close to the part with the unknown electron density and far from that of the known electron density thus making the phase rate of change of the unknown scattering factor to be slow in comparison to that of the known part. In the present study we located the origin close to the top of the grown film. In the case of a buried layer system such as AlAs in GaAs the origin is placed in the AlAs layer far from the GaAs surface. The exact location of the origin is not critical. For example, we found empirically that changing the choice of origin by 20% of the film thickness did not significantly affect the electron density results.

The effectiveness of this procedure can be tested in the following way. To qualify as a real electron density, the function obtained from the Fourier transformation of the complex scattering factor function must satisfy certain constraints: It must be real and positive definite and it should go to zero outside the film. In general the function obtained from the Fourier transformation of the CSF will not strictly satisfy

these constraints. So to test how good is the result we obtained we first impose the constraints by zeroing out all the negative parts and the parts that are clearly outside the film. We then use the resulting electron density function to calculate the diffraction intensities along the Bragg rods. If the agreement with the measured intensities is not satisfactory one can use the newly obtained electron density as the new reference electron density and reiterate the entire procedure to obtain a better result. It turns out that, in the present case, no iterations ns were necessary.

In general epitaxial systems are not fully periodic in 2D with a period equal to the underlying substrate period. Epitaxial systems may have a different commensurate period, may be locally incommensurate with the substrate, or may be nonuniformly strained. A commensurate structure with a different period will give rise to scattering along additional Bragg rods and local incommensurability and non uniform strain give rise to diffuse scattering throughout reciprocal space. Thus, important information about the system is contained in the diffuse scattering intensity function. In this work we only consider x-ray scattering along the substrate-derived Bragg Rods. This provides the folded electron density[1] discussed in the next paragraph and, as shown further below, it provides detailed structural information on the GaAs:Gd_2O_3 system.

Let us now consider the scattering along the substrate defined Bragg rods. Notice that, since the substrate is periodic in 2D and the epitaxial film is chemically bonded to it, the scattering factors along the substrate defined Bragg rods have the form of a delta function in two dimensions. To calculate these scattering factors we divide the system into substrate defined unit cells; however, because of the deviations from the substrate defined 2D periodicity, the electron density is different in different unit cells. The electron density of such a system can be expressed as $\rho(x,\vec{R}_{i,j}+\vec{r})$, where x is the coordinate perpendicular to the interface, $\vec{R}_{i,j}$ is the in-plane position of the (i,j) unit cell and $\vec{r}$ is the in-plane position within the unit cell. Notice, that since the system is not strictly 2D periodic ρ varies with (i,j). The complex scattering factor $T_{\eta,\zeta}$ along the Bragg rod is proportional to the Fourier transform of the electron density

$$T_{\eta,\zeta}(k)\propto\int_V d^2r\,dx\sum_{i,j}\rho(x,\vec{R}_{i,j}+\vec{r})\exp\{i[(\vec{R}_{i,j}+\vec{r})\cdot\vec{k}_{\eta,\zeta}+kx]\},\tag{6}$$

where the summation over i,j is carried over all 2D unit cells.

Since $\vec{k}_{\eta,\zeta}$ is a Bragg rod vector, $\vec{R}_{i,j}\vec{k}_{\eta,\zeta}=2\pi n$. Thus, Eq. (6) reduces to the form

$$T_{\eta,\zeta}(k)\propto\int_V d^2r\,dx\exp\{i[\vec{r}\cdot\vec{k}_{\eta,\zeta}+kx]\}\sum_{i,j}\rho(x,\vec{R}_{i,j}+\vec{r}),\tag{7}$$

namely, the scattering factor along the Bragg rods is the Fourier transform of $\Sigma_{i,j}\rho(x,\vec{R}_{i,j}+\vec{r})$. We shall refer to this as the electron density of the folded system and it is obtained by moving all atoms into one 2D substrate defined unit cell using 2D unit cell vectors. Thus, in spite of local incommensurability, non uniform strain and other deviations from the substrate defined 2D periodicity, the complex scattering factors along the substrate defined Bragg rods are the Fourier transform of a well defined real space electron density, namely, the folded electron density. We can therefore use the method we described before to determine the complex scattering factors along the Bragg rods and determine the folded electron density by Fourier transformation. The folding in the present case is discussed in more detail in Sec. V.

III. SAMPLE PREPARATION AND SAMPLE PROPERTIES.

The samples were prepared at Bell Labs, Lucent Technologies, using precleaned epi ready (100) GaAs wafers specified to have a low crystalline miscut angle $<0.50°$. The GaAs and oxide deposition were done in two separate molecular beam epitaxy (MBE) growth chambers, one for GaAs growth and the other for depositing oxide, linked together by a transfer module with a background pressure of 6×10^{-11} Torr.[7,25]. The transfer process has been evaluated and there is no evidence for oxygen contamination. Inside the MBE chamber, the GaAs wafer was first heated to 580–600°C in an As flux to remove the native oxide from its surface. GaAs deposition was then done using pyrolytic boron nitride effusion cells for the elemental Ga and As. The deposition rate was approximately 0.75–1.0 μ/h and 0.3–0.5 μm of GaAs was deposited. Once the growth of the GaAs was completed, the wafer was transferred to the second MBE chamber for depositing the oxide. Before the oxide growth, the GaAs surface was heated up to $\sim$600°C to remove some As from the surface in order to be gallium stabilized (i.e., contains at least 70% more Ga than As atoms). The resulting (4×6) surface reconstruction is assumed to promote single domain growth because it removes the twofold degeneracy of aligning the (110) Gd_2O_3 plane of rectangular symmetry onto the square symmetric GaAs (100) surface. It was shown that an arsenic stabilized surface, with its associated (2×4) reconstruction, also works but the surplus arsenic is more volatile. As described in Ref. 10, the gadolinium oxide was deposited from a powder-packed source using electron beam evaporation. The substrate temperature was held at 550 °C and the deposition rate was about 0.1 μm/h. During deposition, *in situ* reflection high-energy electron diffraction (RHEED) was used to monitor the growth process. Analysis of the twofold symmetric RHEED patterns indicated that the Gd_2O_3 film is (110)-oriented and grows as a single domain. To check the extent of the single-domain orientational epitaxy the sample was rastered through the incident beam and the orientation of the diffraction pattern was determined to remain unchanged. X-ray diffraction[19] and secondary electron imaging[20] have confirmed that under the growth conditions described above, Gd_2O_3 grows as a cubic single crystal single-domain film.

IV. MEASUREMENT OF THE DIFFRACTION INTENSITY ALONG THE BRAGG RODS

The measurement of the diffraction intensities along the Bragg rods was done in the usual way and is schematically

shown in Fig. 1(a). The sample was mounted at the center of a six circle goniometer and had four rotational degrees of freedom while the detector had 2. The incident beam impinged on the sample surface. As one can easily see from the schematic drawing of the Bragg rods in reciprocal space, the measurement of the diffraction intensity along a Bragg rod is achieved by rotating the sample around an axis perpendicular to its surface and by moving the detector to the position where the diffracted beam is expected to be.

Measurement of the diffraction intensities along Bragg rods requires precision in several ways. The scan must reliably be made along the Bragg rod and not fall off to the sides. The relative intensities along the rod and among different rods must be quantitatively correct to within a few percent. The background from scattering processes not associated with the diffraction along the Bragg rods must be subtracted. To address these needs we have developed a new LABVIEW based software package that controls the goniometers we used and the entire experimental system. The software system includes the geometry code and is capable of controlling both eulerian and kappa type six-circle goniometers. Huber eulerian and Newport kappa goniometers were used. For our application, as described below, the LABVIEW program has distinct advantages over popular goniometer control programs such as SPEC. To obtain reliable control of the goniometers we have measured the orientation of the various rotation axes relative to each other. This was done using an autocollimator mounted on the detector arm and a mirror mounted at the sample position. Once the rotation axes are correctly determined the autocollimator and the mirror must remain aligned with respect to each other under arbitrary rotations around an arbitrary axis. In both goniometers used the orientation of the rotation axes have been found to deviate from orthogonality in some cases by more than 1.5 mrad. Note that for the kappa goniometer, the kappa angle is measured. After determining the rotation axes vectors and adding the corrections to the software control program, the misalignment between the autocollimator and the mirror did not exceed 400 μrad.

We used an incident beam with 10 keV photon energy, chosen because it is approximately the largest energy that is still safely below the absorption edges of all the relevant constituents, thus eliminating fluorescence. The incident beam was focused vertically to about 100 microns, slitted down horizontally to 0.5 mm, and its orientation relative to the goniometer axes was determined to within 100 μrad and inserted into the system control software. The sample was mounted on the goniometer in such a way that the goniometer center of rotation was located at the sample surface and the incident beam impinged on the sample at this same point. A number of Bragg reflections were used to determine the orientation of the reciprocal GaAs unit cell. Any other Bragg point was then found to be within 2 mrad of the corresponding calculated values. This is not enough to guarantee accurate rod scans. We therefore carried out scans perpendicular to the rods at several points along each rod and used the corrections to improve the accuracy. The corrections reduced the errors to less than 200 μrad which is small compared to the detector acceptance angle of 3 mrads. These errors also cause negligible inaccuracy in the position along the Bragg rods.

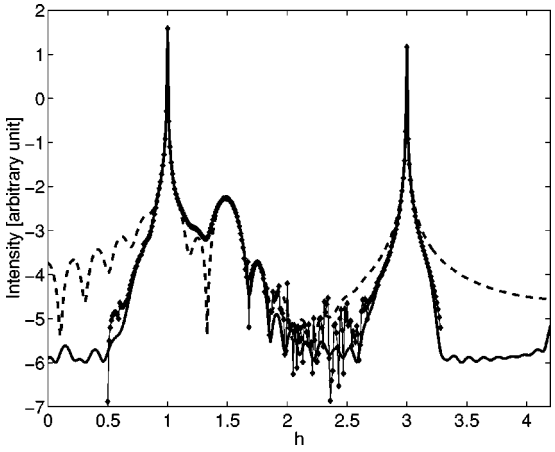

FIG. 3. Diffracted beam intensity in log scale along the $[h1-1]$ Bragg rod. The abscisa is in reciprocal lattice cell units. 10^{-6} has been added to the intensity to avoid negative values in the logarithm. Notice that the Cobra calculated and measured intensities are in very good agreement wherever the signal to noise ratio is large. Dotted curve: experimental results; dashed curve: the initial model; solid curve: COBRA calculation.

In these measurements we purposely used relatively wide slits, 3×3 mm at a distance of 1000 mm from the sample. We did this in spite of the fact that this somewhat increased the background for two reasons. (a) With narrow slits the intensity calibration can be less reliable especially if the incident beam is not quite uniform in intensity. Inaccurate intensity calibration will affect regions of both low as well as high intensities and will therefore have serious adverse effects on the resulting electron density. (b) In case the crystal is slightly miscut so that the surface normal is not exactly along a high symmetry crystallographic axis the Bragg rods will split into a number of parallel but non overlapping Bragg rods each going through one Bragg point. We have shown mathematically, consistent with previous work, that if the miscut is ideal (namely, the terraces are of equal width), the sum of the intensities of all rods at any given k along a Bragg rod is equal to the intensity at that point of a nonmiscut sample. Thus using relatively large slits we automatically add up the contributions of the most relevant split Bragg rods.

The diffracted beam intensity was measured using a plastic scintillator photomultiplier detector operating in current mode with a stable dc preamplifier. The advantage of this detection scheme in comparison to photon counting is its linear response up to at least several hundred thousand photons per second. The dark noise was usually about 3 orders of magnitude smaller than the largest intensity along the Bragg rod contributed by the Gd_2O_3 film. We used an automatic calibrated filter unit to measure the intensities very close to the Bragg peaks. The incident intensity was measured by an ionization chamber located just before the sample. We took precautions to make sure that the entire incident beam measured by the reference detector contributed to the diffraction and the entire diffracted beam was

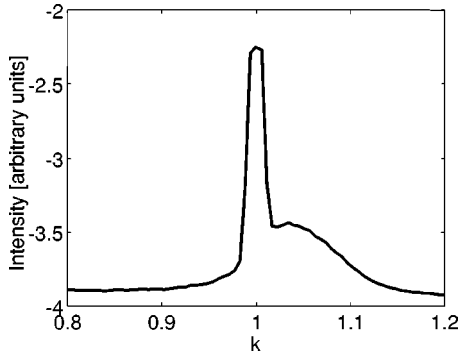

FIG. 4. Diffraction intensity in along the $[1.48\ \zeta-\zeta]$ line.

measured by the signal detector. This requirement was difficult to satisfy when the incidence angle was below 5°, namely, in measurements along the $[h00]$ Bragg rod for $h<1$.

Finally, the background was removed by installing, in front of the signal detector, a paddle which had two types of openings: a $3\times3\ \mathrm{mm}^2$ opening to let the diffracted beam of about $1\times1\ \mathrm{mm}^2$ through and a set of two $3\times2\ \mathrm{mm}^2$ openings separated by a 3 mm blocking region to stop the signal and let the background through. At each point along the Bragg rod a motor moved the paddle to measure the signal and background. The total scan time per Bragg rod amounted to about 2 h. Lastly, the data were corrected for Lorentz and polarization factors.

V. EXPERIMENTAL RESULTS

As explained further below, the range in reciprocal space where the diffraction intensities were measured is limited and the electron density is obtained by Fourier transforming the complex scattering factors in this limited range. To minimize the effect of the missing regions we multiplied all the

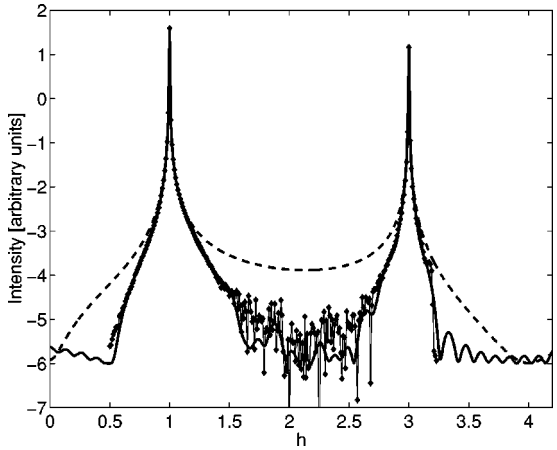

FIG. 5. Diffracted beam intensity in log scale along the $[h11]$ Bragg rod. The abscisa is in reciprocal cell units. 10^{-6} has been added to the intensity to avoid negative values in the logarithm. Notice that the Cobra calculated and measured intensities are in very good agreement wherever the signal to noise ratio is large. Dotted curve: experimental results; dashed curve: the initial model; solid curve: COBRA calculation.

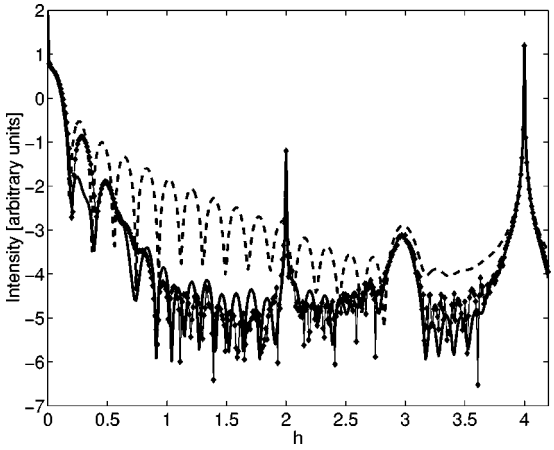

FIG. 6. Diffracted beam intensity in log scale along the $[h0\,0]$ Bragg rod. The abscisa is in reciprocal cell units. 10^{-6} has been added to the intensity to avoid negative values in the logarithm. Notice that the Cobra calculated and measured intensities are in very good agreement wherever the signal to noise ratio is large. Dotted curve: experimental results; dashed curve: the initial model; solid curve: COBRA calculation.

spectra by a Gaussian factor $\exp(k^2\sigma^2/2)$ with $\sigma=0.3$ Å. This has the effect of convoluting the electron density with a Gaussian. The normalized diffraction intensities along the $[h1-1]$ Bragg rod are shown in Fig. 3. The large peaks correspond to [1 1 -1] and [3 1 -1] Bragg peaks. The broad peak at approximately [1.48 1 -1] and the overtones are due to the Gd_2O_3 film. To verify that this peak is not just the tail

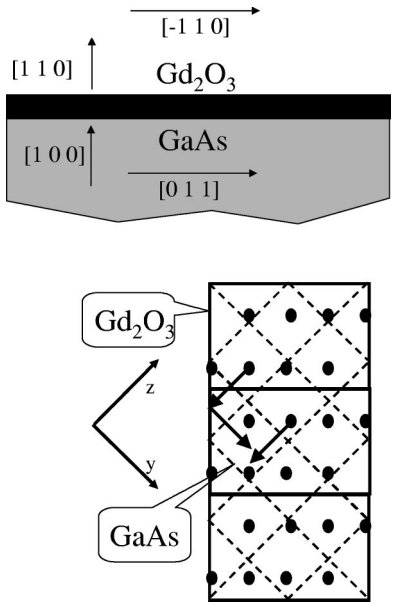

FIG. 7. (a) Top: Crystallographic orientations of the Gd_2O_3 film and the GaAs crystal. (b) Bottom: Gd positions in the first monolayer and the folding procedure using the GaAs 2D reciprocal unit cell vectors marked by the arrows. The Gd_2O_3 cell is represented by the solid rectangles. The short side is the Gd_2O_3 unit cell edge. The long side is the unit cell face diagonal. The dashed squares represent the GaAs 2D unit cells. The mismatch in the vertical direction is -1.9% while the mismatch in the horizontal direction is 4.1%.

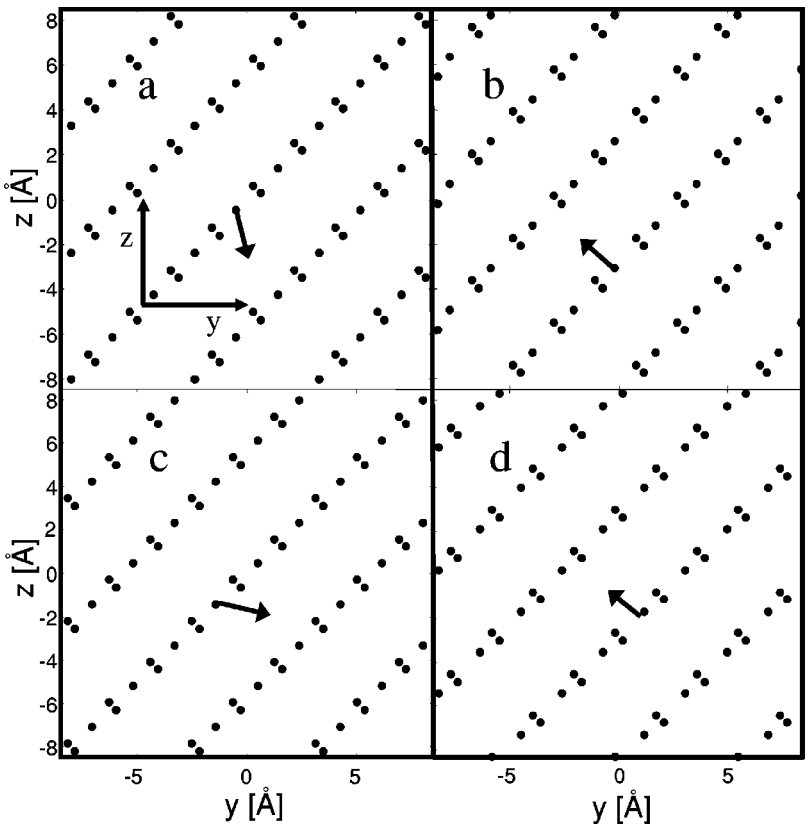

FIG. 8. In-plane folded Gd positions in four consecutive layers of Gd_2O_3. Each square represents 3×3 GaAs 2D unit cells. The structure repeats itself every four layers. Notice that these displays are rotated 45° relative to Fig. 7(b).

of a larger peak at a position off the Bragg rod we performed scans perpendicular to the rod. In GaAs reciprocal lattice coordinates bulk Gd_2O_3 would have a Bragg peak at approximately [1.48 1.04 -1.04]. The diffraction intensity along the $[1.48\ \zeta\ -\zeta]$ line that goes through this point is shown in Fig. 4. As seen the system has indeed a broad peak at that position but it has a much larger peak on the Bragg rod, namely, at [1.48 1 -1]. The diffraction intensities along the $[h-11]$ Bragg rod were found to be equal to within the experimental accuracy to those on $[h1-1]$ while those on $[h11]$, shown in Fig. 5, were completely different. These results confirm the conclusion of Kortan *et al.*[19] that the system is a single crystal with a single domain having 180° rotational symmetry but no 90° rotational symmetry.

The 10 keV incident beam allowed us to measure all the Bragg rods within the range $|k|\leqslant3$; $|l|\leqslant3$ and $0.1<h\leqslant3.5$ (along the $[h00]$ rod, h extended to 4.2). The diffraction intensities along rods with $k+l$ odd were too small to be measured. So the total number of symmetry inequivalent rods that were measured was 13. The $[h00]$ Bragg rod scan shown in Fig. 6 and the $[h1-1]$ scan displayed clearly identifiable Gd_2O_3 contributions. The other Bragg rods also have intensity contributions from the Gd_2O_3 : GaAs interference, but they are weaker.

VI. COMPLEX SCATTERING FACTORS AND STRUCTURE DETERMINATION

As explained in Sec. II the first step is to choose a known structure that is similar to the structure of the system under investigation. We chose to construct a simple model of the system. This model consists of the semi-infinite GaAs crystal and a cubic single domain Gd_2O_3 film on top of it, with the features found by Kortan *et al.*;[19] namely, that the Gd_2O_3 $\langle110\rangle$ axis is perpendicular to the (100) GaAs substrate, the Gd_2O_3 $\langle001\rangle$ axis coinciding with the GaAs $\langle011\rangle$ axis and the orthogonal Gd_2O_3 $\langle1-10\rangle$ axis coinciding with the GaAs $\langle0-11\rangle$ axis. The model further assumes in accordance with the results of Kortan *et al.* that three Gd_2O_3 unit cell edges match four GaAs unit cell face diagonals and one Gd_2O_3 face diagonal matches two GaAs face diagonals. The Gd and O atoms lie approximately in layers parallel to the interface, each layer containing both Gd and O atoms. The largest vertical distance between Gd atoms within one layer is 0.457 Å as compared to the 1.92 Å interlayer separation in bulk Gd_2O_3. Four such layers contain all the atoms of one unit cell. We shall concentrate our discussion mainly on the Gd atoms, which dominate the scattering. The oxygen atoms cannot be clearly seen because they have only eight electrons in comparison to 64 for Gd.

One such layer is schematically shown in Fig. 7. In this figure and throughout the rest of the paper whenever we refer to bulk Gd_2O_3 we mean bulk Gd_2O_3 strained to be exactly commensurate with the underlying GaAs. Since the period of the Gd_2O_3 is not equal to that of the underlying GaAs, the COBRA analysis will yield the folded structure where all the atoms of the combined cell are folded into one GaAs unit cell. Examples of the folding process are schematically indicated in Fig. 7. The folded structures of four consecutive monolayers can be seen in Fig. 8. The dots represent the in-plane positions of the Gd atoms folded into a single GaAs unit cell. Each dot of a pair represents two folded atoms at

slightly different heights and each single dot represents four folded atoms also of slightly different heights, which are superposed on top of each other in this projection.

Before applying the COBRA procedure, we attempted a traditional least squares fit with nine parameters. These include an overall intensity factor, a factor u_r multiplying the Gd_2O_3 repeat distance perpendicular to the surface and the number of monolayers *n*. Due to the mismatch between the film and the substrate (-1.9% in the $\langle 001 \rangle$ direction and 4.1% in the $\langle 1-10 \rangle$ direction) the atomic positions will be displaced in a disordered fashion from their ideal positions. We assumed that the distribution about their ideal positions is Gaussian with a width σ. We used three such parameters: σ_{ga} for the GaAs substrate, and σ_{yz} and σ_x for the distribution in the Gd_2O_3 film plane and perpendicular to it. Finally, three additional parameters were used to translate the film relative to the substrate in the *x*, *y*, and *z* directions.

The initial model parameters were first refined by best fitting the Bragg rod diffraction intensities. The results were as follows: $u_r = 0.946$, $n = 16$, $\sigma_{ga} = 0.35$ Å, $\sigma_{yz} = 0.93$ Å, and $\sigma_x = 0.98$ Å. The film displacement parameters were found to be such that the ridges of the folded Gd atom positions in the first Gd_2O_3 monolayer overlap the positions of the Ga or As atoms at the top substrate layer. The fits were found to be insensitive to the motion of the film parallel to the ridges. This is a result of the fact that due to the large σ_{yz} the electron density along the ridges varies very little.

The quality of the model was checked by comparing the diffraction intensities calculated from this model with the experimental results. As seen in Figs. 3, 5, and 6 the agreement is rather poor. This is true also of all other rods. It is therefore clear that this initial model is indeed inadequate. Following the procedure discussed in Sec. II we used the complex scattering factors obtained from the model as the known reference scattering factors *S* and calculated the amplitude and phase of the unknown scattering factors *U* and of the total scattering factors *T*. The measurements were limited to $h > 0$ because when $h < 0$ the diffracted beam goes into the substrate. The complex scattering factors for $h < 0$ were calculated from the general relation that the scattering factor at $\vec{k}$ is equal to the complex conjugate of the scattering factor at $-\vec{k}$. The scattering factors of the unknown part vary smoothly across the Bragg points so they could be obtained near the Bragg points by interpolation. The interpolation was carried out in the range $(h_b - 0.05) < h_b < h_b + 0.05$, where h_b is the *x* component of a Bragg point. After applying the constraints discussed in Sec. II, we used the resulting electron density to calculate the diffraction intensity along the Bragg rods. The results are shown in Figs. 3, 5, and 6. Notice that, in contrast to the model, the results obtained from the COBRA analysis are in very good agreement with experiment over two orders of magnitude below the intensity of the largest Gd_2O_3 feature.

To check the effect of the iteration procedure we carried out one iteration. We used the newly obtained electron density as the new reference electron density and then proceeded as before to obtain a new electron density and to calculate the scattering intensity along the Bragg rods. We show as an example one Bragg rod in Fig. 9 and, as seen, the agreement between the iterated structure and experiment has improved a little. Similar small improvements were observed in all other Bragg rods, but the electron density did not significantly change.

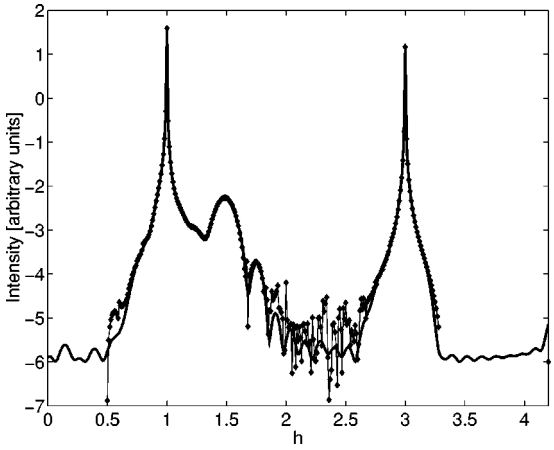

FIG. 9. Diffracted beam intensity in log scale along the $[h1-1]$ Bragg rod. 10^{-6} has been added to the intensity to avoid negative values in the logarithm. Notice that the Cobra calculated and measured intensities are in very good agreement wherever the signal to noise ratio is large. Dots: experiment; solid curve: COBRA calculation after one iteration.

VII. THE ATOMIC STRUCTURE

Before interpreting the electron density function, in terms of the atomic structure, we need to take several considerations into account. First, the range in reciprocal space where we have data is approximately seven reciprocal lattice units. This means that the narrowest features possible in the electron density function will have a half width equal to the GaAs unit cell divided by two times the reciprocal range, namely, 0.35 A. In calculating the Fourier transform we increased the range in reciprocal space by a factor of 3, padding the extra range with zeros. This increased the point

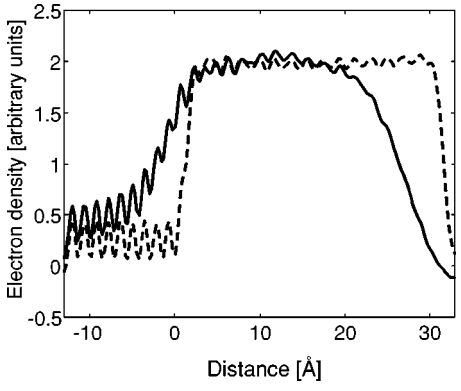

FIG. 10. Average layer electron density as a function of distance from interface. Dashed: initial model; solid: COBRA calculation. The nominal interface is at zero. The electron density to the left represents Ga and As layers, to the right it represents Gd layers with a small oxygen contribution.

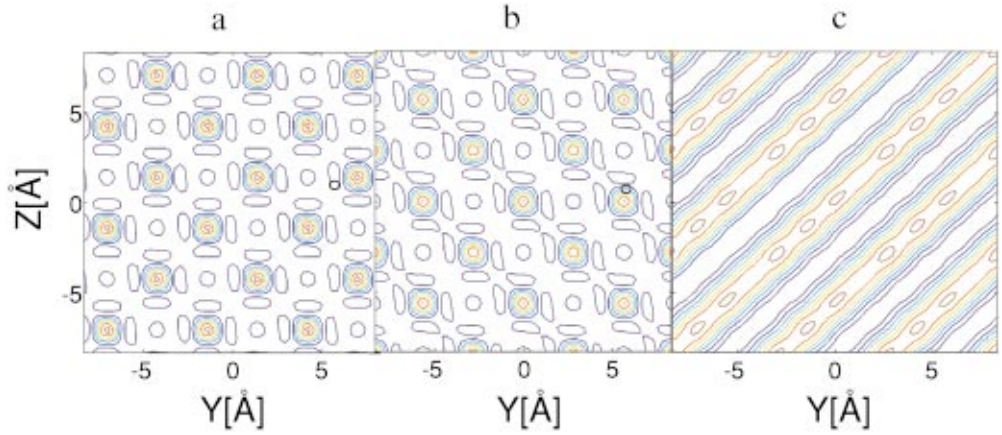

FIG. 11. (Color) In-plane electron density maps. Each map consists of 3×3 GaAs 2D unit cells. (a) COBRA calculated map of layer -8. (b) COBRA calculated map of layer -7. (c) Initial model calculated map of layer $+9$. Warm colors represent high density. Cold colors represent low density.

density in the electron density function but of course it did not increase the resolution. Second, regions of the film which are completely incommensurate with the substrate give rise, when folded, to a uniform electron density. The portion of the film that is incommensurate may vary as a function of the distance from the interface. Other contributions to a background electron density may be due to inaccuracies in the phase and possibly other sources.

The in-plane averaged electron densities obtained from the model and COBRA calculations are shown in Fig. 10. The nine peaks on the left correspond to 9 monoatomic layers of Ga and As. Ga and As cannot be distinguished easily because their atomic numbers differ only by 2. The larger electron density on the right corresponds to sixteen Gd_2O_3 monolayers. In the starting model we assumed an abrupt change from GaAs to Gd_2O_3 and an abrupt termination of the film. The COBRA electron density shows that the transition is gradual over approximately five layers. The transition region may be either a result of interface roughness or Gd diffusion into the GaAs. The fact that the surface roughness is also about five layers suggests, that the transition region is a result of interface roughness. We suggest that the GaAs substrate had probably about five layers of roughness to begin with. The overall width of the epilayer measured at the mid transition points is 27 Å.

Notice that on the left, far from the interface within the GaAs substrate, the peak to valley ratio in the COBRA calculated electron density is large and corresponds to a Gaussian distribution $A\exp[-x^2/(2\sigma^2)]$ with $\sigma=0.35$ Å. As pointed out, this is the minimal value expected since the data extends to a limited range in reciprocal space. Going to the right into the Gd_2O_3 film, the peak to valley ratio decreases

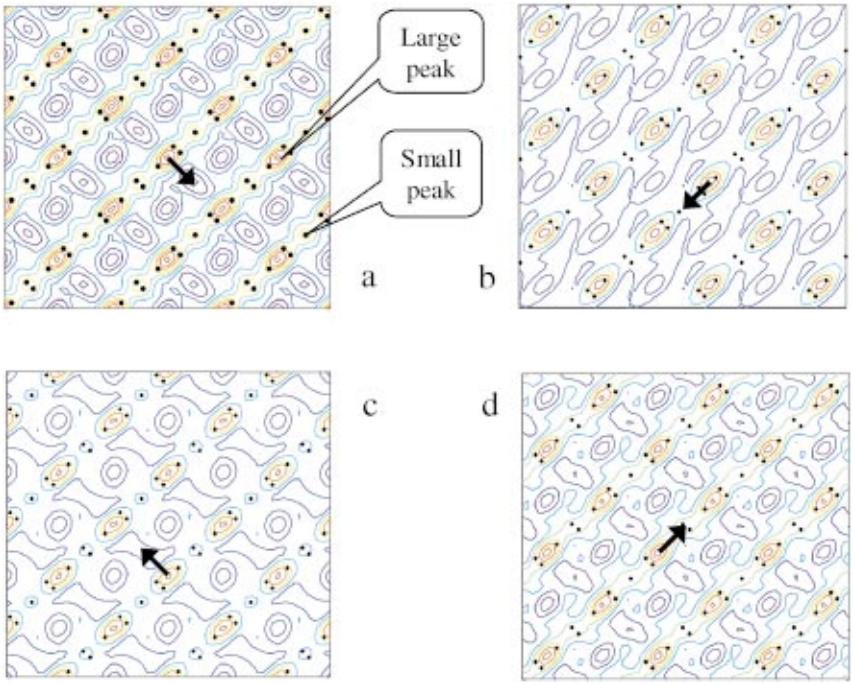

FIG. 12. (Color) In-plane electron density maps of layers 9 through 12. Each map consists of 3×3 GaAs 2D unit cells. Notice that shifting the electron density map in one layer by a vector represented by the arrow yields approximately the electron density map in the next layer.

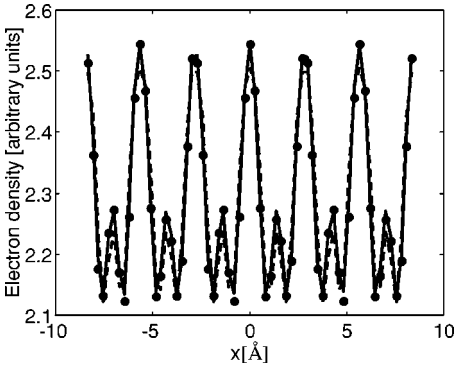

FIG. 13. Fits to the electron density along a ridge in layer 9. Dots: experiment; dashed curve: fit without background; solid curve: fit with background.

leading to an increase of σ. The peak to valley ratio in the Gd_2O_3 film is about equal to that of the initial model. So, $\sigma \approx 0.9$ Å. This value is much larger than the resolution and is presumably a result of the nonuniform strain present in the film.

Let us now consider the in-plane structure. The in-plane electron density map of layers -8 and -7 are shown in Figs. 11(a) and 11(b). The layers are numbered with respect to the nominal GaAs/Gd_2O_3 interface with negative numbers on the GaAs side of the interface. In both layers the Ga and As atomic positions can be clearly seen and the two maps are shifted with respect to each other as expected for GaAs. The Gaussian half width of these peaks is 0.37 Å, namely, resolution limited and similar to the vertical width.

An example of the model electron density map on the Gd_2O_3 side (nominally layer $+9$) is shown in Fig. 11(c). This map shows the ridges and valleys expected from the folded Gd positions shown in Fig. 8. However, the electron density along the ridges is almost completely flat. In contrast, the COBRA calculated electron density shown in Fig. 12 shows clear structure along the ridges. To understand this structure we show on the same figure the Gd positions in bulk Gd_2O_3 as black dots. As described in Sec. VI, each dot in a pair of dots represents two atoms folded to the same place in the plane but at slightly different positions perpendicular to the plane. Similarly each single dot represents four occluded atoms. The smaller peaks along the electron density ridges coincide with the positions of one dot or one pair of dots namely with four folded atoms as expected. On the other hand the large elongated peaks appear in the middle between a pair and a single dot. This suggests that the folded atoms in the real system are actually closer together than expected from the Gd_2O_3 bulk structure. This behavior is seen in all layers.

To determine the distances of the real system folded atomic positions from the peak positions we have plotted the electron densities along the ridge centers. An example is shown in Fig. 13. We then fitted the electron density with Gaussian functions. Each group of four folded atoms was represented by a Gaussian. The amplitudes and widths of all Gaussians were assumed to be equal and were allowed to vary together with the distances of the Gaussians from the nearest large electron density peaks. This gave us three variable parameters. Using these parameters we could obtain good fits to the electron density distributions. However, since we expect also possible electron density background we fitted the data also with a constant electron density background as the fourth parameter. These refinements gave excellent fits. The distances and the Gaussian widths are shown in Fig. 14 as a function of layer number. Since both fits were good the values shown in the figure are the averages of the parameters obtained in both fits and the error bracket is the average difference between the two. The two horizontal bars on the right represent the distances in alternate layers in the bulk Gd_2O_3 crystal. Thus the results show that in the first three layers the in-plane folded positions of each group of eight atoms coincides with the center position of a large peak in the electron density. As the distance from the interface increases, the distances increase towards those present in bulk Gd_2O_3. Using a similar approach we have found that the Gaussian widths in the in-plane direction perpendicular to the ridges is also $\sigma \approx 0.65$ Å. Notice that while these values are smaller than the values in the initial model, they are still much larger than the resolution meaning that the system has relatively large disorder both parallel and perpendicular to the ridges.

The fact that the folded in-plane electron density is not completely uniform means that the epilayer is at least partially commensurate with the substrate. The fact that GaAs and bulk Gd_2O_3 lattices are not exactly matched means that the epilayer is strained and the presence of a large disorder means that the strain is partially relaxed. It should be emphasized that the Gd displacements near the interface, discussed in the previous paragraph, are not manifestations of strain. By strain we usually mean that the unit cell dimensions change but the atoms within it retain their relative positions. This is not the case here; the displacements are not simply the result of a contraction or an expansion of a unit cell.

Now we discuss the stacking of the Gd_2O_3 and show that it follows that of GaAs and not that of bulk Gd_2O_3. The repeat distance in the vertical direction is four layers in both GaAs substrate and Gd_2O_3 film. Let us consider the four consecutive layers shown in Fig. 8. Notice that the in-plane atomic positions in each layer are shifted relative to the next layer by a vector indicated in the layer. These vectors are $a(0.08\vec{I}_y - 0.42\vec{I}_z)$, $a(-0.25\vec{I}_y + 0.25\vec{I}_z)$, $a(0.42\vec{I}_y - 0.08\vec{I}_z)$, and $a(-0.25\vec{I}_y + 0.25\vec{I}_z)$. Here a is the GaAs unit cell, and $\vec{I}_y$ and $\vec{I}_z$ are unit vectors in the y and z directions. The COBRA calculated electron densities in four consecutive layers shown in Fig. 12 are also related to each other in a similar way but the shift vectors are different. They are $a(0.25\vec{I}_y - 0.25\vec{I}_z)$, $a(-0.25\vec{I}_y - 0.25\vec{I}_z)$, $a(-0.25\vec{I}_y + 0.25\vec{I}_z)$, and $a(0.25\vec{I}_y + 0.25\vec{I}_z)$. This shows that the stacking order in the film is different from the stacking order in bulk Gd_2O_3. The difference in the stacking order can also be seen in the following way: In Fig. 8 the center point in map (a) is on a ridge, in (b) on a valley, in (c) on a ridge and in (d) on a valley. In contrast the sequence in Fig. 12 is (a) ridge, (b) valley, (c) valley, (d) ridge. The stacking order shown in Fig. 12 is valid throughout the entire film thickness. The fact that the stacking order in the film is different from that in the

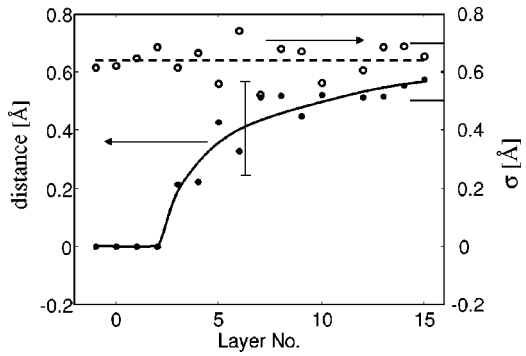

FIG. 14. The distance between Gaussian peak and the neighboring large electron density peak (dots) and Gaussian width (circles) as a function of layer number. The curves are guide to the eye.

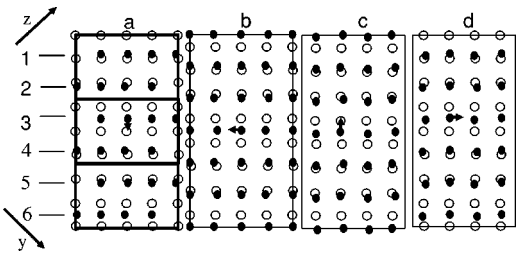

FIG. 15. The unfolded in-plane Gd positions in four consecutive layers shown as dots. Notice that the positions in one layer can be approximately obtained from the positions in the previous layer by shifting them by the vector shown in that layer. (The last vector on the right shifts the positions from the last layer to the first). The circles represent Ga and As positions in four consecutive layers of GaAs.

bulk is unusual but not unheard of. For example, Lamelas *et al.*[26] have found that the stacking order, in Co and Cu in Co/Cu superlattices grown on GaAs, is different from the corresponding bulk structures.

The COBRA determined Gd positions in the unfolded structure of four layers are shown in Fig. 15. As in the folded structure, the atomic positions in adjacent layers are shifted with respect to each other by the vectors shown in each layer. The atoms in rows 3 and 6 fold into the small peaks in the folded electron density maps whereas the atoms in rows 1, 2, 4, and 5 fold to positions on either side of the large peaks. In this figure we also show the Ga and As positions (open circles) in four consecutive monolayers of GaAs. The interesting point is that the relative positions of the Gd and Ga/As positions remain approximately the same in all layers. This relation is not present in bulk Gd_2O_3.

The distances shown in Fig. 14 can be schematically seen in Fig. 15. These are the distances of the Gd atoms in rows 1, 2, 4, and 5 relative to the neighboring Ga/As positions. As mentioned before, these distances are zero within our experimental accuracy in the first 3 Gd_2O_3 layers, namely the Gd positions in these rows overlap the Ga/As positions. As the distance from the interface increases, they move away towards the bulk Gd_2O_3 positions.

VIII. SUMMARY AND CONCLUSIONS

In this paper we have shown that the COBRA method provides a detailed 3D electron density map of a rather complex epitaxial system. It is important to emphasize that the electron density we obtained is qualitatively different from the initial model we started with. Furthermore, the very good agreement obtained between the calculated and measured diffraction intensities along thirteen symmetry inequivalent Bragg rods is not a result of fitting but comes from the determination of the complex scattering factors. In fact the simple model we started with turned out to be both qualitatively and quantitatively wrong; yet, the final COBRA result is very close to the correct electron density as evidenced from the fact it yields diffraction intensities that are in very good agreement with experiment. The final results did not depend sensitively on the specific initial model we chose as long as the intensities it yields are of the same order of magnitude as the experimentally measured ones. We believe this is quite generally true on the basis of many simulations that we did, in addition to the measurements reported here.

The electron density we have obtained is that of the folded system. It provides the atomic positions averaged over all 2D unit cells as well as the position probability distribution function, namely, the probability to find an atom at a certain position. In the present case and in many other cases the relation between the folded and unfolded systems is quite transparent. So, one can easily draw conclusions about the unfolded system. The folded structure does not contain information about structural correlations such as pair correlations, the average coherence length of locally incommensurate regions, etc. For example, if two adjacent atoms in the unit cell have a certain distribution width, the distance between them in the real system may have a much smaller distribution if their positions are correlated or up to two times larger if their positions are anticorrelated. So, other experimental methods are needed to complement COBRA. Information on correlations can be obtained from diffuse scattering outside the Bragg rods, from XAFS, PDF, and possibly x-ray holographic methods. However, as mentioned before the information they provide is averaged over atoms of the same species at inequivalent positions throughout the epitaxial film. The information we now have on the epitaxial Gd_2O_3 film can be summarized as follows.

(a) As suggested by Kortan *et al.*,[19] the film structure is cubic and single domain with the $\langle 110 \rangle$ axis of the Gd_2O_3 perpendicular to the surface and its $\langle -110 \rangle$ and $\langle 001 \rangle$ axes parallel to the GaAs $\langle 011 \rangle$ and $\langle 0-11 \rangle$ axes, respectively.

(b) At the interface the electron density changes gradually from the GaAs to the Gd_2O_3 over four to five layers. The transition region is probably due to interface roughness. A similar transition region is seen at the surface and is probably due to surface roughness. The fact that the two thicknesses are about equal suggests that the GaAs had this surface roughness to begin with.

(c) The nonuniform strains due to the mismatch between the GaAs and Gd_2O_3 unit cells and their partial relaxation introduce disorder in the folded atomic positions. The distribution width in the GaAs is much smaller than the parallel and perpendicular widths in the Gd_2O_3 film. This is expected

in a thin film. It is interesting that the perpendicular width is larger than the in-plane one.

(d) The Gd positions in the first few layers are displaced so as to exactly match the positions of the underlying Ga and As. As the distance from the interface increases they relax to the bulk Gd_2O_3 positions.

(e) The stacking order of the layers in the film is different from that in bulk Gd_2O_3. In fact the main peaks of the folded electron density in each monolayer of the film are exactly at the Ga and As positions in the GaAs and follow the same stacking order.

The last two points indicate that Gd_2O_3 tends to adopt a structure similar to that of GaAs. This could be at the bottom of the fact that Gd_2O_3 forms a very good passivation layer for GaAs.

ACKNOWLEDGMENTS

Y. Yacoby is grateful for the opportunity to spend a sabbatical year at the university of Washington. This project was supported by the US-Israel Bi-National Science Foundation under Contract No. 1999-187. M. Sowwan is grateful for the financial support of the Israel ministry of Science and Technology. Work at the University of Washington and PNC-CAT was supported by DOE Grants No. DE-FG03-98ER45681 and DE-FG03-97ER45628. Work at MHATT-CAT was supported by the U.S. Department of Energy, Grant No. FG02-99ER45743. Use of the Advanced Photon Source was supported by the U.S. Department of Energy, Basic Energy Sciences, Office of Energy Research, under Contract No. W-31-109-Eng-38. One of us (R.C.) acknowledges support from the NSF Frontiers of Physics Center, FOCUS.

*On sabbatical at Physics department, University of Washington, Seattle, WA 98195; Electronic address: yizhak@vms.huji.ac.il

[1] Y. Yacoby, R. Pindak, R. MacHarrie, L. Peiffer, L. Berman, and R. Clarke, J. Phys.: Condens. Matter **12**, 3929 (2000).
[2] A. Revesz and K. Zaininger, J. Am. Ceram. Soc. **46**, 606 (1963).
[3] O. Weinreich, J. Appl. Phys. **37**, 2924 (1966).
[4] T. Mimura, K. Odani, N. Yokoyama, Y. Nakayama, and M. Fukuta, IEEE Trans. Electron Devices **25**, 573 (1978).
[5] W.T. Tsang, Appl. Phys. Lett. **33**, 426 (1978).
[6] C.W. Wilmsen, *Physics and Chemistry of III-V Compound Semiconductor Interfaces* (Plenum, New York, 1985), p. 403.
[7] M. Hong, M. Passlack, J.P. Mannaerts, J. Kwo, S.N.G. Chu, N. Moriya, S.Y. Hou, and V.J. Fratello, J. Vac. Sci. **14**, 2297 (1996).
[8] M. Passlack, M. Hong, J.P. Mannaerts, R.L. Opila, S.N.G. Chu, N. Moriya, F. Ren, and J.R. Kwo, IEEE Trans. Electron Devices **44**, 214 (1997).
[9] J. Kwo, M. Hong, A. R. Kortan, D. W. Murphy, J. P. Mannaerts, A. M. Sergent, Y. C. Wang, and K. C. Hsieh, in *Compound Semiconductor Surface Passivation and Novel Device Processing*, MRS Symposia (Materials Research Society, Warrendale, PA 1999), p. 57.
[10] M. Hong, J. Kwo, A.R. Kortan, J.P. Mannaerts, and A.M. Sergent, Science **283**, 1897 (1999).
[11] M. Hong, Z.H. Lu, J. Kwo, A.R. Kortan, J.P. Mannaerts, J.J. Krajewski, K.C. Hsieh, L.J. Chou, and K.Y. Cheng, Appl. Phys. Lett. **76**, 312 (2000).
[12] E.J. Nelson, J.C. Woicik, M. Hong, J. Kwo, and J.P. Mannaerts, Appl. Phys. Lett. **76**, 2526 (2000).
[13] S.K. Sinha, M.K. Sanyal, S.K. Satija, C.F. Majkrzak, D.A. Neumann, H. Homma, S. Szpala, A. Gibaud, and H. Morkoc, Physica B **198**, 72 (1994).
[14] P. F. Miceli, *Semiconductor Interfaces, Microstructures and Devices: Properties and Applications* (IOP Publishing, Bristol, UK, 1993), p. 87.
[15] J. Zegenhagen, Surf. Sci. Rep. **18**, 7 (1993).
[16] I.K. Robinson and D.J. Tweet, Rep. Prog. Phys. **55**, 599 (1992).
[17] D.C. Joy, D.E. Newbury, and D.L. Davidson, J. Appl. Phys. **53**, R81 (1982).
[18] M. Tegze and G. Faigel, Nature (London) **380**, 49 (1996).
[19] A.R. Kortan, M. Hong, J. Kwo, J.P. Mannaerts, and N. Kopylov, Phys. Rev. B **60**, 10 913 (1999).
[20] B. Bolliger, M. Erbudak, M. Hong, J. Kwo, A.R. Kortan, and J.P. Mannaerts, Surf. Interface Anal. **30**, 514 (2000).
[21] X. Torrelles, J. Rius, F. Boscherini, S. Heun, B.H. Mueller, S. Ferrer, J. Alvarez, and C. Miravitlles, Phys. Rev. B **57**, R4281 (1998).
[22] J. Rius, C. Miravitlles, and R. Allmann, Acta Crystallogr., Sec. A: Found. Crystallogr. **52**, 634 (1996).
[23] X. Torrelles, J. Rius, M. Pedio, R. Felici, P. Rudolf, J. Alvarez, S. Ferrer, and C. Miravitlles, Phys. Status Solidi B **215**, 773 (1999).
[24] D.K. Saldin, R. Harder, H. Vogler, W. Moritz, and I.K. Robinson, Comput. Phys. Commun. **137**, 12 (2001).
[25] M. Hong, J. Cryst. Growth **150**, 1 (1995).
[26] F.J. Lamelas, C.H. Lee, H. Hui, W. Vavra, and R. Clarke, Phys. Rev. B **40**, 5837 (1989).